PNAS RESEARCH ARTICLE | NEUROSCIENCE

The nonclassical MHC class I Qa-1 expressed in layer 6 neurons regulates activity-dependent plasticity via microglial CD94/NKG2 in the cortex

Ioana A. Marin[a,b], Alan Y. Gutman-Wei[a,b], Kylie S. Chew[a,b], Aram J. Raissi[a,b], Maja Djurisic[a,b], and Carla J. Shatz[a,b,1]

Contributed by Carla J. Shatz; received March 7, 2022; accepted April 20, 2022; reviewed by Michael Greenberg and Jonathan Kipnis

During developmental critical periods, circuits are sculpted by a process of activity-dependent competition. The molecular machinery involved in regulating the complex process of responding to different levels of activity is now beginning to be identified. Here, we show that the nonclassical major histocompatibility class I (MHCI) molecule Qa-1 is expressed in the healthy brain in layer 6 corticothalamic neurons. In the visual cortex, Qa-1 expression begins during the critical period for ocular dominance (OD) plasticity and is regulated by neuronal activity, suggesting a role in regulating activity-dependent competition. Indeed, in mice lacking Qa-1, OD plasticity is perturbed. Moreover, signaling through CD94/NKG2, a known cognate Qa-1 heterodimeric receptor in the immune system, is implicated: selectively targeting this interaction phenocopies the plasticity perturbation observed in Qa-1 knockouts. In the cortex, CD94/NKG2 is expressed by microglial cells, which undergo activity-dependent changes in their morphology in a Qa-1–dependent manner. Our study thus reveals a neuron–microglial interaction dependent upon a nonclassical MHCI molecule expressed in L6 neurons, which regulates plasticity in the visual cortex. These results also point to an unexpected function for the Qa-1/HLA-E (ligand) and CD94/NKG2 (receptor) interaction in the nervous system, in addition to that described in the immune system.

neuronal MHCI | corticothalamic neurons | ocular dominance plasticity | microglial innate immune receptor

Significance

Molecules regulated by neuronal activity are necessary for circuits to adapt to changing inputs. Specific classical major histocompatibility class I (MHCI) molecules play roles in circuit and synaptic plasticity, but the function of most members of this family remains unexplored in brain. Here, we show that a nonclassical MHCI molecule, Qa-1 (H2-T23), is expressed in a subset of excitatory neurons and regulated by visually driven activity in the cerebral cortex. Moreover, CD94/NKG2 heterodimers, cognate receptors for Qa-1, are expressed in microglia. A functional interaction between Qa-1 and CD94/NKG2 is necessary for regulating the magnitude of ocular dominance plasticity during the critical period in the visual cortex, implying an interaction in which activity-dependent changes in neurons may be monitored by microglia.

In the cerebral cortex, neural activity during developmental critical periods is required for remodeling synapses and shaping circuits (1–4). For example, in the visual system, activity-dependent circuit refinement is initially regulated by spontaneously generated activity and then later relies on external stimuli driving activity along the visual pathways (1, 5, 6). Many lines of experiments demonstrate that specific sets of activity-regulated molecules, along with cellular mechanisms of synaptic plasticity, contribute and indeed are required for circuits to adapt and remodel, both by strengthening some connections and by weakening and pruning away others.

In an unbiased in vivo screen for genes regulated by spontaneously generated neural activity in the visual system, two classical major histocompatibility class I (MHCI) molecules, well-known for their immune system function, were found to be regulated by neural activity, expressed in neurons, and located at synapses (7–10). The MHCI locus in the mouse (and human) contains 50+ genes encoding both classical MHCIs, such as H2-Db and H2-Kb, and many nonclassical MHCIs (11–13). In KbDb knockout (KO) mice, synapses are not pruned and plasticity is altered, both in the lateral geniculate nucleus (LGN) and the visual cortex (8, 14, 15). Other immune molecules, such as complement components expressed in neurons and microglia, have also been implicated in synapse pruning (4, 16). Astrocytes are thought to participate as well (17, 18). As more molecular components for synapse pruning and remodeling are identified in glia and neurons (19–21), a "neuroimmune system architecture" is emerging.

While the expression and function of classical MHCI molecules in the healthy brain have been the subject of several studies, to date nothing is known about the neural function of nonclassical MHCIs, although expression has been noted in previous studies or in RNA sequencing databases (10, 22–24). Here, we investigate the expression and function of a nonclassical MHCI, Qa-1 (H2-T23), in the healthy brain. In the immune system, Qa-1 (as well as its human homolog HLA-E) is known for roles in infectious and autoimmune disease, including experimental autoimmune encephalitis (EAE), by interacting with receptors on natural killer (NK) cells and T cells (25–27). Using in situ hybridization, qRT-PCR, and Ribotagging, we find that Qa-1 expression within the cortex is highly restricted to layer 6 (L6) cortical neurons. By comparing wild-type (WT) and Qa-1 KO mice in the

Author contributions: I.A.M., K.S.C., A.J.R., M.D., and C.J.S. designed research; I.A.M., A.Y.G.-W., K.S.C., A.J.R., and M.D. performed research; I.A.M., A.Y.G.-W., K.S.C., A.J.R., and M.D. analyzed data; and C.J.S. wrote the paper.

Reviewers: M.G., Harvard Medical School; and J.K., Washington University School of Medicine in St. Louis.

Competing interest statement: I.A.M. and J.K. were coauthors of a previous article: *J. Exp. Med.* 2018 Jun 4; 215(6):1627–1647. doi: 10.1084/jem.20180247. Epub 2018 Apr 11.PMID: 29643186.

[1]To whom correspondence may be addressed. Email: cshatz@stanford.edu.

This article contains supporting information online at http://www.pnas.org/lookup/suppl/doi:10.1073/pnas.2203965119/-/DCSupplemental.

Published June 1, 2022.

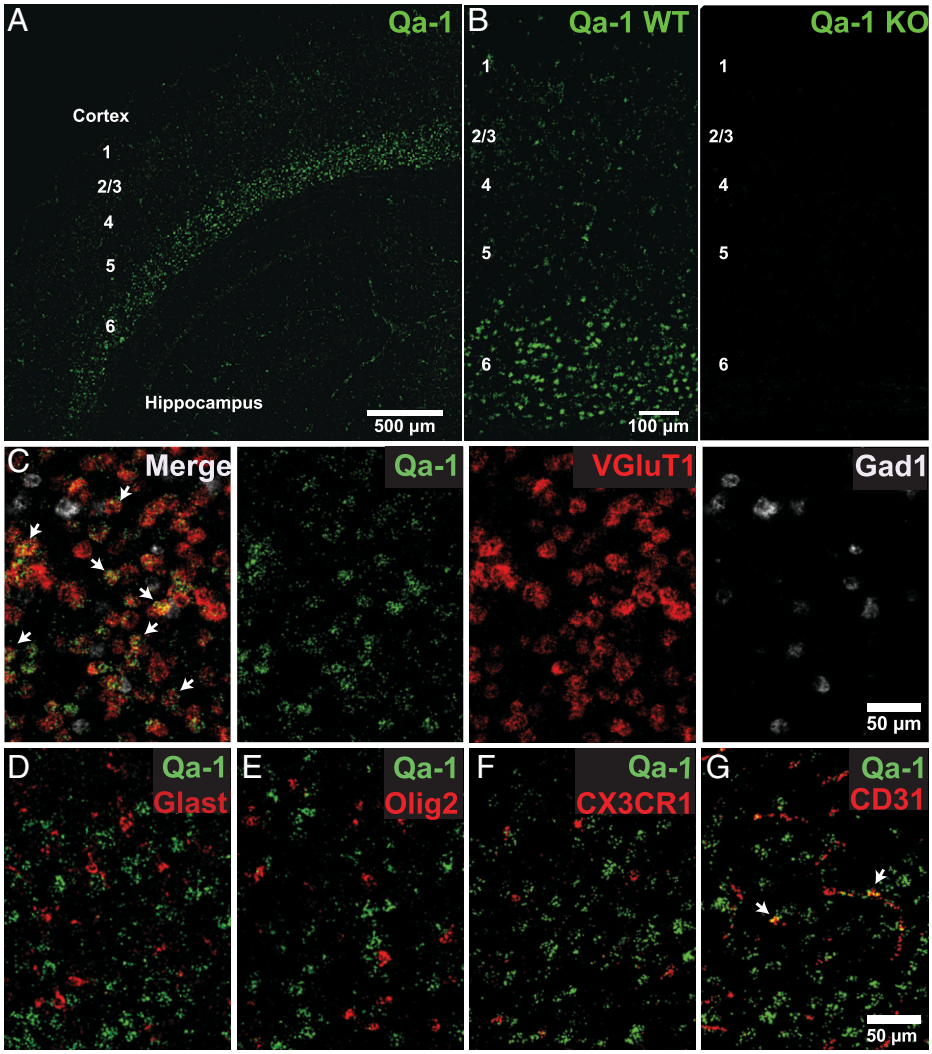

Fig. 1. Qa-1 mRNA is highly expressed in layer 6 (L6) cerebral cortical excitatory neurons in the healthy brain. RNAscope in situ hybridization for Qa-1 (H2-T23) mRNA at P45. (*A*) Low power view of the visual cortex (coronal section, medial is to the *Right*). (*B*) Higher power view of specific Qa-1 signal (*Left*), compared with Qa-1 KO control (*Right*). Numbers mark cortical layers. (*C*) Multiplex RNAscope in situ hybridization for Qa-1 combined with excitatory (VGlut1) or inhibitory (Gad1) neuronal markers at P45. Arrows mark examples of dual labeling (yellow) of Qa-1 (green)-positive cells with vGlut1 (red) but not GAD1 (white) (merge). (*D*–*F*) Dual RNAScope in situ hybridization for Qa-1 mRNA and glial markers, as follows: (*D*) astrocytes, Glast; (*E*) oligodendroglia, Olig2; (*F*) microglia, Cx3cr1; and (*G*) endothelial cells, CD31, a subset colabeled with Qa-1 (examples marked with arrows).

well-established paradigm of eye closure to manipulate visual activity, we explore a role for Qa-1 function in the circuit-level readout of ocular dominance (OD) plasticity during the visual cortical critical period. A transgenic line that bears a point mutation in Qa-1 known to abrogate the interaction with NKG receptors (26) is also studied here, leading us to discover Qa-1-dependent functions of microglia both in vivo and in vitro.

Results

The Nonclassical MHCI Qa-1 Is Expressed in Layer 6 Cortical Neurons in the Healthy Brain. To evaluate the expression pattern of Qa-1 messenger RNA (mRNA) in the brain, we performed in situ hybridization using RNAscope technology. An intense Qa-1 signal with a cellular pattern is detected primarily in L6 of the neocortex (Fig. 1 *A* and *B*), with lower levels and more diffuse puncta in upper cortical layers. Almost no signal can be found in the hippocampus or other subcortical areas. The specificity of the in situ probe was validated in the cortex of Qa-1 KO animals, where no signal was detected (Fig. 1*C*). To assess the identities of cells expressing Qa-1, multiplex RNAscope was carried out with neuronal (VGluT1, Gad1), glial (Glast, Olig2, CX3CR1), or endothelial (CD31) cell markers in combination with Qa-1 (Fig. 1 *C*–*G*). Strong colocalization is present between Qa-1 and VGlut1, a marker for excitatory pyramidal neurons, in L6. No coexpression of mRNA could be detected for inhibitory neurons (Gad1) or glial markers. Occasional colocalization of Qa-1 mRNA with the endothelial marker CD31 (Fig. 1*G*) was observed. These results suggest that, within the brain parenchyma, Qa-1 is primarily expressed in excitatory pyramidal neurons in the cerebral cortex. While there have been no previous studies examining the cell-type specificity of Qa-1 expression, our results are also consistent with expression data reported in various RNA sequencing databases from unperturbed brain tissue (i.e., NucSeq [28–30] or Ribotag [10, 24]).

Qa-1 mRNA Is Enriched in the Synaptic Compartment and Is Associated with Ribosomes from Cortical Neurons. L6 of the neocortex receives input from the thalamus and is composed of the following two main types of excitatory neurons classified based on their axonal projection patterns (Fig. 2*A*): corticothalamic (CT) pyramidal neurons (the majority of cells) and local,

cortico-cortical (CC) neurons (31–33). CT neurons send a characteristic feedback projection to the thalamus and also send extensive recurrent axons to layers 5 and 4. CT neurons are selectively labeled in an Ntsr1 BAC-Cre transgenic line, facilitating identification (neurotensin receptor 1 [24, 34]). Via their axonal projections, L6 CT neurons are well positioned to modulate neural activity in many cortical layers as well as in the thalamus.

To assess if Qa-1 mRNA is present in this subset of L6 excitatory neurons, Ntsr1-Cre Ribotag mice were generated (24, 34, 35). In this line, L6 Ntsr1-Cre-expressing neurons carry the ribosomal protein (Rpl22) tagged with hemagglutinin (HA) (36). Immunoprecipitation (IP) of ribosomes from cortical homogenates with an antibody against HA then yields ribosome-associated transcripts specifically from L6 CT neurons, providing information about the transcriptome as well as the translatome. The specificity of Cre-targeting was confirmed by immunohistochemistry for HA expression; HA immunostaining is confined exclusively to cortical L6 cells, as expected (Fig. 2*B*). Next, to assess if Qa-1 mRNA is expressed in the CT subset of L6 neurons, multiplex RNAscope was performed for Qa-1 and Cre mRNA in the cortex of Ntsr1-Cre Ribotag mice; many cells colocalize the two signals, which is consistent with CT subtype identity (Fig. 2*C*).

To obtain information about the subcellular distribution of Qa-1, several approaches were used. First, we reasoned that if Qa-1 is similar to many synaptic molecules (37–39) the mRNA might be transported and targeted to axon terminals. Consequently, the mRNA might be detected by qRT-PCR not only in the cortex but also in the thalamus (the main projection of L6 CT neurons), which is what is observed (Fig. 2*D*). Second, previous studies of classical MHCI molecules have shown that they are located at synapses (8, 9). Therefore, synaptosomes were prepared from cortical lysates. Not only is Qa-1 mRNA specifically detected (Fig. 2 *E* and *F*), but also expression is greatly enriched compared with whole lysate and cytosolic fractions (Fig. 2*G*; Qa-1 mRNA could not be detected in similar preparations from Qa-1 KO cortex). Finally, to verify that the presence and enrichment of Qa-1 mRNA derives from neuronal, and specifically from L6 neurons, the Ribotag method was used to IP HA-tagged ribosomes from the Ntsr1-cre Ribotag whole cortex and from synaptic fractions. Qa-1 mRNA is enriched in L6 CT neurons compared with whole lysate and even further enriched in HA IPs from synaptosome preparations (Fig. 2*H*). Because Ribotag IPs significantly enrich for ribosome-associated transcripts that are in the process of being translated (36, 40), these observations are consistent with the suggestion that Qa-1 transcripts may be locally translated in the synaptic compartment of L6 neurons.

Expression of Qa-1 in Layer 6 Is Developmentally Regulated and Activity Dependent. Molecules that are synaptically localized and translated are frequently regulated by neuronal activity (37, 39). To examine this possibility for Qa-1, in situ hybridization was used to examine mRNA in L6 neurons of the visual cortex at various stages of postnatal development, when visual experience drives patterns of neuronal activity necessary for circuit refinement (1–3). To monitor Qa-1-expressing L6 cells belonging to the population of excitatory pyramidal neurons, sections were also probed for VGluT1, and the percentage of VGluT1-expressing neurons coexpressing Qa-1 was assessed at each age. Prior to eye-opening and the onset of vision, Qa-1 mRNA cannot be detected. Following eye opening, Qa-1 levels increase between postnatal day 20 (P20) and P35, corresponding to the visual cortical critical period (41–44). Adult levels are reached by P45, when roughly 70% of VGluT1 neurons in L6 express Qa-1 (Fig. 3*A*). To examine if perturbations in visual experience may affect Qa-1 expression, juvenile mice were dark reared for 10 d during the visual critical period (Fig. 3*B*). Immediately at the end of the dark exposure protocol, Qa-1 mRNA expression is significantly lower than in normally reared (NR) animals. However, the restoration of vision in ambient light for 5 to 10 h is sufficient to recover expression (Fig. 3 *C* and *D*). This result indicates that visual experience during the critical period is necessary to achieve adult levels of expression of Qa-1, consistent with the idea that Qa-1 is an activity-dependent gene.

OD Plasticity Is Perturbed in the Visual Cortex of Mice Lacking Qa-1. Molecules regulated by visually driven activity are frequently also required for cellular and system-level mechanisms of neuronal plasticity (10, 45–47). To test if this is the case for Qa-1, OD plasticity was assessed in Qa-1 KO vs. WT mice during the visual cortical critical period. Qa-1 KO mice are healthy when maintained in a pathogen-free facility and are not immune compromised (25, 26). In addition, somatic expression of Qa-1 mRNA is detected only in cortical neurons, and we have determined that the formation of the retinogeniculate projection and remodeling to yield the eye-specific layers in the LGN are intact (*SI Appendix*, Fig. S1).

The OD plasticity paradigm measures the visual cortical response to changes in binocular balance in a circuit that intimately involves both L4 and L6; Qa-1 expressing L6 CT neurons in the visual cortex send descending axons to LGN neurons in the thalamus and also receive monosynaptic inputs from LGN neurons. L6 CT neurons also send ascending axon collaterals to synapse on L4 and L5a neurons, establishing a thalamus-L6-L4 circuit that has been studied extensively in many species including mouse (Fig. 2*A*) (31, 33, 48). During the critical period, neurons require visually driven inputs from both eyes to establish and maintain binocularity. If one eye is closed even briefly during this period, functional inputs driven by the open eye expand their territory to dominate neurons in the binocular zone, while inputs from the closed eye weaken and are pruned (Fig. 4*A*); this use-dependent takeover is called OD plasticity (2, 3, 49, 50).

OD plasticity was induced in WT vs. Qa-1 KO mice by monocular visual deprivation (MD) for 4 d from P28 to P32 (Fig. 4*A*), a time of peak sensitivity during the critical period. The magnitude of plasticity was assessed in the cortex by measuring the expansion in width of the representation of the open eye using induction of the immediate early gene Arc. Arc mRNA is up-regulated within minutes of visual stimulation (42), has been used as a readout of functional connectivity in many studies (8, 51–53), and has been validated as a reliable indicator of changes in binocularity using intrinsic signal optical imaging (41, 43, 54). Following 4 d MD, in situ hybridization was used to examine the spatial pattern of Arc mRNA up-regulation in L4 or L6 cortical neurons ipsilateral to the open, stimulated eye (Fig. 4*B*). The binocular zone in the hemisphere ipsilateral to the open eye was assessed because in NR animals, the ipsilateral eye representation is highly restricted (*SI Appendix*, Fig. S2*A*).

In WT animals, studies have shown that, following MD, the deprived eye input to cortical neurons rapidly weakens, followed a few days later by strengthening of the open eye input (55, 56). In NR animals, the ipsilateral eye representation is comparable between Qa-1 WT and KO mice (*SI Appendix*, Fig. S2 *A* and *B*). Following 4 d of MD, Arc induction

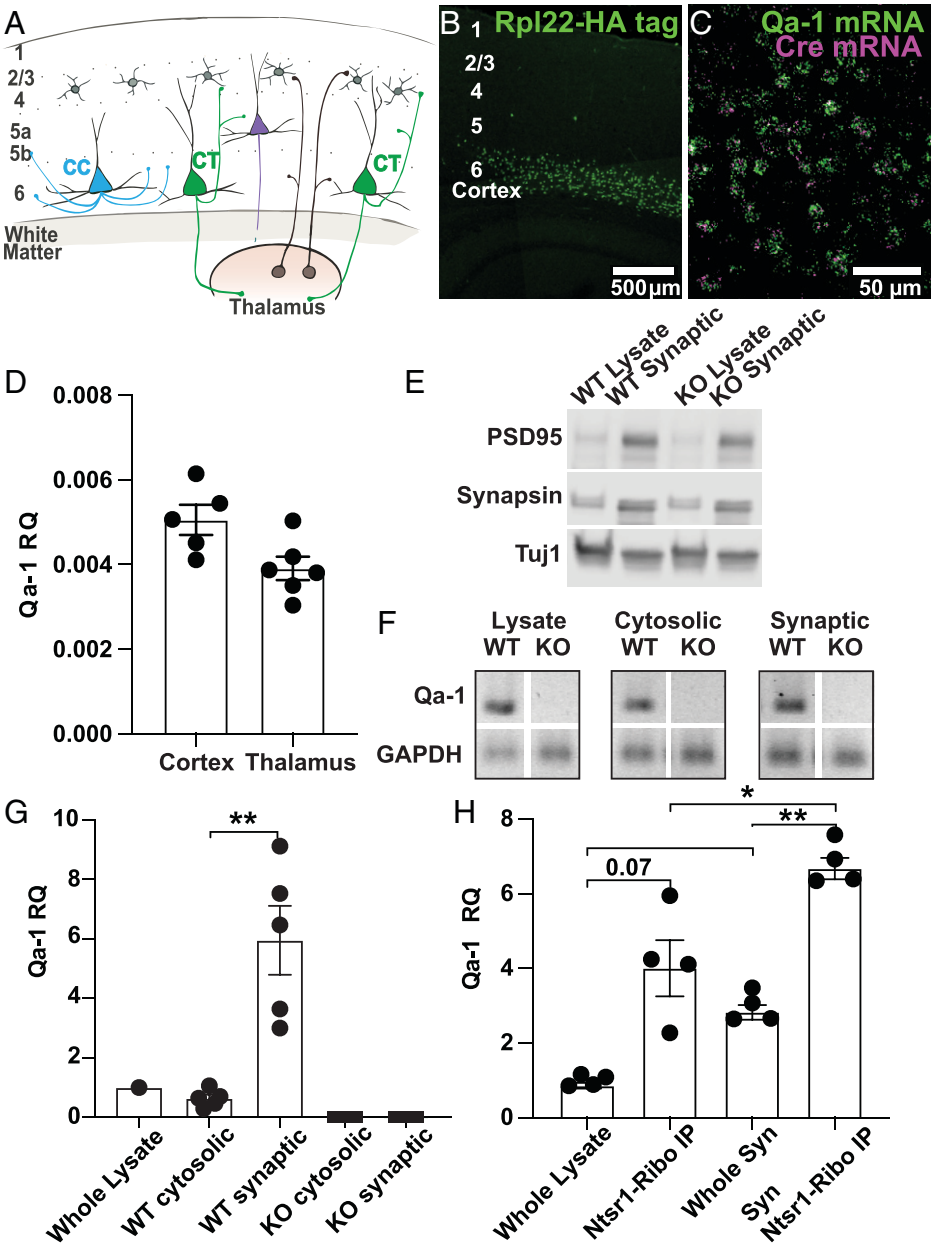

Fig. 2. Qa-1 transcript is enriched in the synaptic compartment of L6 neurons and is associated with translation machinery. (*A*) L6 circuit diagram showing the two main types of L6 excitatory neurons and their projections; CC neurons (blue) confine their axons within the cortex; CT neurons (green) send a descending axonal projection to the thalamus and recurrent collaterals to L5 pyramidal cells (purple) as well as to L4 neurons (gray). (*B*) Immunofluorescence for HA tag expressed in Ntsr1-Cre x Ribotag cortex. Ntsr1 marks the subset of L6 CT neurons (green in *A*). (*C*) Dual RNAscope in situ hybridization for Qa-1 mRNA (green) and Cre mRNA (magenta) in L6 of the cortex. Cre expression is driven under the Ntsr1 promoter. Many cells are double labeled. (*D*) qRT-PCR quantification of Qa-1 expression in the cortex and dorsal thalamus, which contains axons from L6 CT neurons ($n = 5$ animals). (*E*) Western blot of cortical lysate and synaptic fractions from Qa-1 WT and Qa-1 KO probed for synaptic proteins PSD95 and Synapsin1, showing enrichment of these markers in the synaptic fraction. (Tuj1 is a neuronal marker expected to be present in all fractions). (*F*) Representative gel electrophoresis of qPCR end products from reactions probing for Qa-1 mRNA (*Top*) and GAPDH mRNA (*Bottom*) in whole cortical lysates and cytosolic, and synaptic fractions from Qa-1 WT and KO mice. (*G*) qRT-PCR quantification of Qa-1 expression in the following different fractions of the cerebral cortex from Qa-1 WT versus KO: whole lysate ($n = 1$ for reference) and cytosolic fraction and synaptic fraction ($n = 5$ animals). Note an enrichment of Qa-1 mRNA in synaptic fraction and no signal detected in any fraction of Qa-1 KO. (*H*) qRT-PCR quantification of Qa-1 mRNA expression in the following different fractions of the cerebral cortex from Ntsr1-Cre x Rpl22-flox mice: whole cortical lysate, cortical lysate fraction IP with the HA tag expressed in Ntsr1-positive neurons (Ntsr1-Ribo IP), whole synaptic fraction (Whole Syn), and synaptic ribosome-bound fraction (Syn Ntsr1-Ribo IP) ($n = 4$ animals/group). Note an enrichment of Qa-1 mRNA in Ntsr1 Ribotag IP and further enrichment in the Ntsr1 Ribotag synaptic IP. qRT-PCR expression levels in *D*, *G*, and *H* are relative to GAPDH, and levels in *G* and *H* are further normalized to whole lysate levels. $^{**}P < 0.01$, $^{*}P < 0.05$, based on one-way ANOVA with Tukey's post hoc.

generates a detectable change in the representation of the open eye in Qa-1 WT mice, while in the Qa-1 KO visual cortex, the same time course results in a much greater increase in the width of the open eye representation, both in L4 and in L6 (Fig. 4*C*). This observation suggests that the mechanisms restricting the extent of open eye strengthening are not properly regulated in the visual cortex of Qa-1 KO mice.

To gain further insight into how Qa-1 may regulate neuronal plasticity, we considered its signaling partners. In the immune system, Qa-1 is known to signal by binding to the receptor family CD94/NKG2, of which members are heterodimers composed of a CD94 molecule and an NKG2 molecule (11, 57, 58) (Fig. 4*D*). In transgenic mice carrying an R72A point mutation in the Qa-1 domain that binds to NKG2 receptors, signaling is

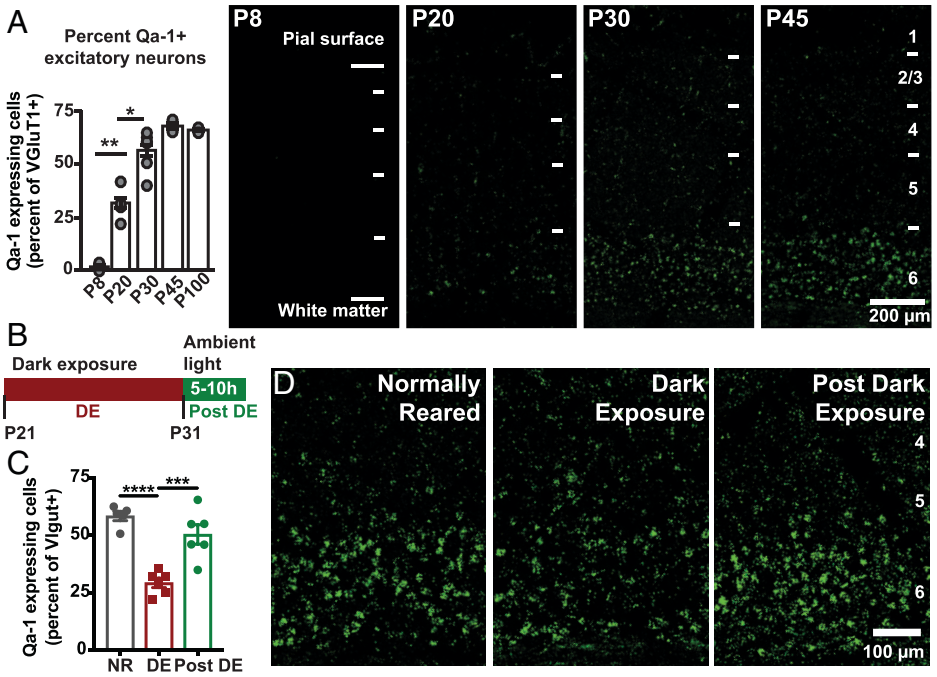

Fig. 3. Qa-1 mRNA expression in L6 visual cortical neurons is activity dependent. (*A*) *Left*, Quantification of Qa-1-expressing excitatory neurons in L6 of visual cortex (as a percentage of VGluT1-expressing cells in L6; dual RNAscope was performed for Qa-1 and VGluT1 as in Fig. 1*C* for quantification purposes). *Right*, RNAscope in situ hybridization for Qa-1 expression in visual cortex across the cortical layers at P8, P20, P30, and P45. Cortical layers are labeled. (*B*) Experimental paradigm for dark exposure during the visual cortical critical period from P21 to P31. (*C*) Quantification of percent Qa-1-expressing cells in L6 at P31 (n = 5 to 6 mice per group) with normal rearing (NR), with dark exposure (DE), and with DE followed by 5- to 10-h restoration of ambient light (Post DE). (*D*) Representative images of RNAscope in situ hybridization for Qa-1 mRNA, relating to *C*. ****$P < 0.0001$, ***$P < 0.001$, **$P < 0.01$, *$P < 0.05$, based on 1-way ANOVA with Tukey's post hoc.

abrogated (Fig. 4*D*) (26). To examine if a similar interaction between Qa-1 and CD94/NKG2 is required in the brain, we assessed OD plasticity in visual cortex of R72A mutant mice. The increase in the width of the open eye representation following MD is significantly greater in R72A mutants than in the WT (Fig. 4*E*), while in R72A animals reared with normal vision, the representation of the ipsilateral eye is comparable to WT (*SI Appendix*, Fig. S2 *A* and *B*). This result phenocopies the observation in Qa-1 KO (Fig. 4 *C* and *E*), suggesting that signaling through CD94/NKG2 is necessary for Qa-1 function.

Qa-1 Receptor Family CD94/NKG2 Members Are Expressed in Microglia. The observation that OD plasticity is also perturbed in the R72A mutant prompted us to search for NKG2/CD94 receptors in the brain. Expression of CD94 mRNA, as well as the NKG2C isoform v1, can be detected using qRT-PCR in whole cortical lysates; NKG2A mRNA is barely detectable (Fig. 5*A*). These results suggest that NKG2C/CD94 may be the dominant form of the receptor in brain. To determine which cell types in the visual cortex might express CD94/NKG2, immunohistochemistry was performed in cortical sections. To our surprise, signal for both CD94 and NKG2 is present in microglial cells scattered throughout the cortex including L4 and L6 (Fig. 5 *B*–*E*).

Since the expression of this heterodimeric Qa-1 receptor in the brain has not been reported previously, several additional approaches were used to verify that microglia express CD94/NKG2. First, microglia were isolated from the cortex using anti-CD11b-conjugated beads (Fig. 5 *F* and *G*) (59), and then the expression of CD94 and NKG2 mRNA isoforms was assessed by qRT-PCR (Fig. 5 *H*–*J*). Expression of CD94 and NKG2C, but not NKG2A, was not only significant but also enriched in the microglial fraction. Finally, microglial expression of NKG2 was confirmed by fluorescence-activated cell sorting (FACS) (Fig. 5*K*) using a pan NKG2 antibody (26, 60). Together, these results are consistent with the suggestion that a subset of microglia express a heterodimeric CD94/NKG2, most likely NKG2C, receptor for Qa-1.

Microglial Engulfment of Synaptosomes In Vitro Is Diminished in the Absence of Qa-1. Microglia are thought to interrogate and engulf synapses (61, 62). Evidence suggests that a variety of molecules, including complement cascade members, CX3CR1, and P2YR12, contribute in part to this process in vitro and/or in vivo (61, 63, 64). To explore if Qa-1 participates in neuron-microglial interactions, the paradigm of in vitro synaptosome engulfment by cultured microglia was employed (65). FACS staining was first used to verify that the majority of microglia in culture, but not astrocytes, express high levels of NKG2 (Fig. 6*A*). Synaptosomes prepared from Qa-1 WT or KO cortex were isolated, labeled with pHrodo, and "fed" to cultured microglia. Engulfment of synaptosomes, as assessed by the amount of pHrodo fluorescence, was approximately 20% greater with synaptosomes prepared from the WT cortex than from Qa-1 KO (Fig. 6 *B* and *C*).

The in vitro approach also permitted us to ask if Qa-1-dependent engulfment requires Qa-1 expression in the microglia, the synaptosomes, or both. We conducted "mix-and-match" experiments in which the same assay was performed but this time pairing Qa-1 KO microglia with synaptosomes from the WT vs. KO cortex. Similar to WT, Qa-1 KO microglia are capable of engulfing WT synaptosomes but fail to engulf as many Qa-1 KO synaptosomes (Fig. 6*D*). Additionally, both WT and KO microglia engulf similar levels of pHrodo-labeled WT synaptosomes (Fig. 6*E*), showing that engulfment depends on the presence of Qa-1 in synaptosomes and is not dependent on Qa-1 expression

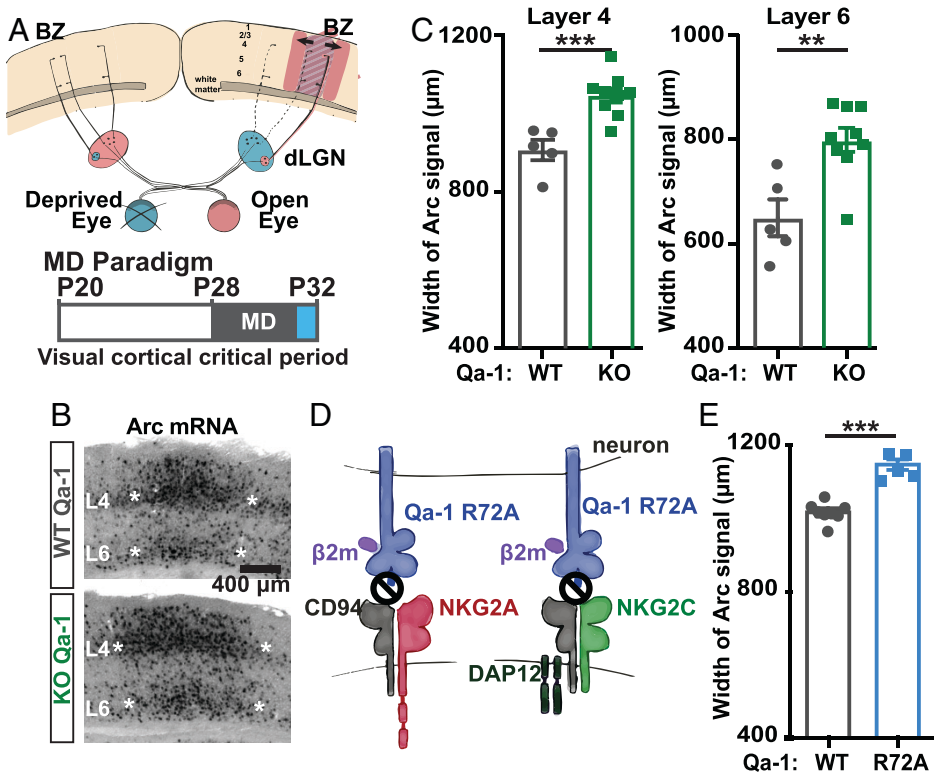

Fig. 4. Excessive open eye strengthening following MD in the visual cortex of Qa-1 KO and in Qa-1 R72A mice. (*A*) OD plasticity experimental paradigm and diagram of connections from open and closed eye to binocular zone (BZ) of the visual cortex. Monocular eye closure from P28 to P32 normally leads to an expansion of the representation of the open eye (arrows: pink) in the visual cortex (ipsilateral to the open eye). In WT and Qa-1 KO mice, one eye was deprived (DE) at P28. At P32, induction of Arc mRNA driven by vision through the open eye, followed by Arc in situ hybridization, was used to assess the cortical territory functionally connected to the open (nondeprived) eye. dLGN, dorsal lateral geniculate nucleus. (*B*) Representative in situ hybridization for Arc mRNA in cortex of WT (*Top*) versus Qa-1 KO (*Bottom*) after 4 d MD. Labeled cells appear black. Asterisks denote limits of intense Arc mRNA signal in L4 and L6 of the BZ. (*C*) Quantification of open eye strengthening assessed by measuring the width of Arc mRNA signal in L4 or L6 in Qa-1 WT versus KO following MD. Note the significant increase (approximately 20%) in the width of open eye representation in Qa-1 KO versus WT, both in L4 and L6. (n = 6 to 8 sections/animal; 5 to 7 animals/group). (*D*) Cartoon showing that the interaction between Qa-1 (with b2m subunit necessary for its expression) and its NKG2 immune receptor family (heterodimers of CD94 and NKG2A or NKG2C, depicted with signaling partner DAP12) is blocked in Qa-1 transgenic mice bearing the R72A point mutation. (*E*) Quantification of open eye strengthening assessed by the width of Arc mRNA signal in L4 in Qa-1 WT versus R72A mutant (NR = reared with normal binocular visual experience). (n = 6 to 8 sections/animal; 7 to 8 animals/group). $^{**}P < 0.01$, $^{***}P < 0.001$, based on *t* tests (*C* and *E*).

in microglia. This finding is consistent with results of Qa-1 expression experiments, of Qa-1 mRNA expression being confined to excitatory neurons (Fig. 1*C*) and enrichment in IPs from synaptosomes prepared from the neuronal Ntsr-1 Ribotag cortex (Fig. 2 *E*–*H*). Together, the observations implicate Qa-1 in synaptosome engulfment by microglia. Given that Qa-1 mRNA is largely expressed in L6 cortical neurons, it is remarkable that a Qa-1 dependent effect on engulfment can even be detected in these assays, in which microglia and synaptosomes are prepared from the entire cortex.

A Microglial Response to Monocular Deprivation Is Absent in the Qa-1 KO Visual Cortex. Previous studies have shown that microglia monitor neuronal activity (66) and can undergo morphological changes in response to changes in activity (63). Monocular deprivation during the critical period leads to rapid (within 12 to 24 h) hyperramification of microglia in the visual cortex ipsilateral to the open eye, which experiences a rapid drop in visually driven activity from the closed, contralateral eye (63). We have already shown that the maintenance of Qa-1 mRNA expression in L6 neurons during the critical period requires vision (Fig. 3 *C* and *D*). To test if just 24 h of eye closure is sufficient to decrease Qa-1 mRNA, monocular deprivation was performed (Fig. 7*A*), which is a procedure that causes a fall in neuronal activity and an imbalance in activity driven by the two eyes in binocular cortical neurons in the visual cortex contralateral to the closed eye (44, 49, 55). To monitor Qa-1 mRNA specifically in L6 CT neurons, the Ntsr1-Cre Ribotag mice were used; a significant decrease was detected in Qa-1 mRNA expression in this subset of L6 cortical neurons contralateral to the deprived eye (Fig. 7*B*).

This rapid fall in neuronal expression of Qa-1 mRNA within 24 h suggests that Qa-1 might contribute to the microglial morphological response to MD. To examine this possibility, one eye was closed at P28, and 24 h later, the ramification of microglial processes was measured in L4 of the binocular zone of the visual cortex in Qa-1 WT and KO. Cortical L4 was chosen to measure the microglial response because it contains both the recurrent axonal projections from L6 CT neurons as well as L6 apical dendrites. In the WT cortex ipsilateral to the open eye, microglia responded to the decrease in activity caused by eye closure with an increase in process ramification (Fig. 7 *C* and *D*, *Top*), as observed previously by Sipe et al. (63). In contrast, in the Qa-1 KO cortex, microglia failed to increase branching 24 h following MD (Fig. 7 *C* and *D*, *Bottom*). At this timepoint, the microglia appear to be unresponsive, suggesting that Qa-1 is required for the microglial morphological response to the effects of monocular deprivation. This requirement for Qa-1 is consistent with our observation that the Qa-1 receptor CD94/NKG2C can be detected in microglia.

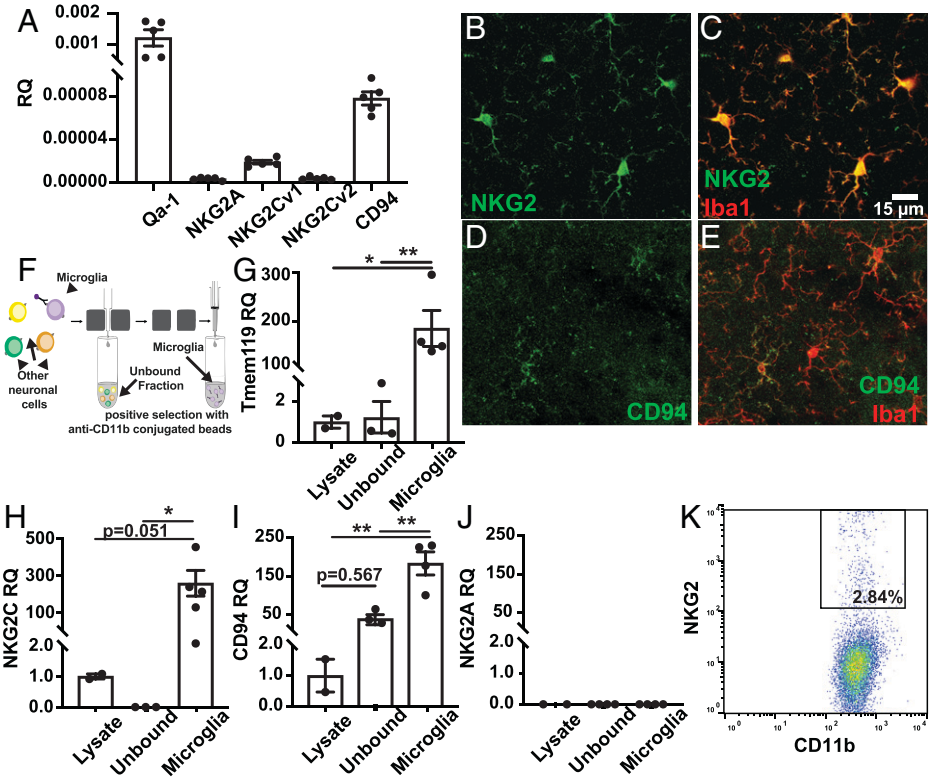

Fig. 5. Microglia express Qa-1 receptors CD94/NKG2 in the cerebral cortex. (*A*) qRT-PCR quantification of expression of Qa-1 and CD94/NKG2 subsets in whole cortical lysates (P75), relative to GAPDH ($n = 5$ animals). Note a significant expression of CD94 and the v1 isoform of NKG2C (NKG2Cv1), required for NKG2C signaling. (*B–E*) Immunohistochemistry for the microglial marker Iba1 (red) combined with NKG2 (green, *B* and *C*) or CD94 (green, *D* and *E*) in cortical sections. Scale bar, 15 µm. (*F*) Diagram of magnetic separation of microglia cells from the cortex (cartoon adapted from Miltenyi), yielding a microglia fraction and an unbound fraction. (*G–J*) qRT-PCR quantification of Tmem119, NKG2C, CD94, and NKG2A expression in the separated fractions, relative to GAPDH and normalized to cortical lysate levels ($n = 2$ to 5 mice per group). (*K*) FACS plot of acutely dissociated adult cortical microglia, identified by marker CD11b expression and stained for NKG2. $^*P < 0.05$, $^{**}P < 0.01$, based on one-way ANOVA followed by Tukey's post hoc.

Discussion

A major finding of this study is the unexpected discovery that Qa-1, a nonclassical MHCI molecule, is present in the cerebral cortex, is expressed in L6 excitatory neurons, is regulated by neural activity, and contributes to sensory-driven plasticity in the visual cortex during the developmental critical period. We have also found that a subset of microglia express CD94/NKG2C, a known receptor for Qa-1 in the immune system (57, 67, 68) but previously not reported to be present in brain. In the visual cortex of transgenic mice carrying a point mutation that blocks binding to CD94/NKG2 (25), sensory-driven plasticity is also altered, arguing for an interaction between Qa-1 on neurons and CD94/NKG2C on microglia. Moreover, in Qa-1 KO mice, cortical microglia in vivo fail to increase ramification in response to changes in sensory-driven activity induced by MD, and in vitro, microglial engulfment of synaptosomes lacking Qa-1 is diminished. Because Qa-1 is primarily expressed in L6 excitatory neurons, these observations collectively imply a specific function for this nonclassical MHCI molecule in activity-dependent plasticity of the cortical circuits in which L6 neurons participate.

Qa-1 Is Likely to Act at the Synapses of L6 Cortical Neurons. Multiple lines of evidence suggest that Qa-1 is predominantly expressed in L6 excitatory neurons. First, in in situ hybridizations, Qa-1 mRNA can be detected in VGluT1, but not GAD1, positive neurons and is not present in any glial cell types (Fig. 1). Secondly, Qa-1 mRNA can be enriched in IPs from the L6 CT cortex, using the Ntsr1-Cre Ribotag mouse line (Fig. 2). We should emphasize here that this cell-type-specific expression is observed in the cerebral cortex of healthy mice maintained in our pathogen-free colony; it is possible that under circumstances of infection and inflammation, the expression pattern of Qa-1 may change.

By using synaptosome preparations, we have also gained further information about the subcellular localization of Qa-1 mRNA; the Qa-1 transcript is enriched almost sixfold in synaptic fractions over a whole lysate prepared from cortical homogenates (Fig. 2 *F* and *G*). Notably, in Ntsr1 Ribotag experiments, Qa-1 transcripts are enriched even further in the IPs from synaptosomes (Fig. 2*H*), suggesting that Qa-1 mRNA may be located at synapses formed by L6 CT neurons. Further study at the ultrastructural level would be helpful in identifying precise subcellular location. The fact that Qa-1 transcript levels are also high in the dorsal thalamus (Fig. 2*D*), the main projection target of L6 CT neurons, suggests a presynaptic presence. It is conceivable that the synaptic fraction might contain mRNA derived from glial cells; however, the enrichment of Qa-1 mRNA after selective IP from Ntsr1-Cre Ribotag mice supports the argument that the majority of Qa-1 transcripts derive from L6 neurons. The Ribotag method yields transcripts associated with the translation machinery (36, 39), suggesting that the Qa-1 protein may also be locally translated at synapses made by L6 CT neurons, as is the case for many other synaptically localized mRNAs (38). Furthermore, Ribotagging also reveals a decrease in ribosome-associated Qa-1 transcripts contralateral to the closed eye 24 h after MD (Fig. 7*B*), suggesting that it is poised to be rapidly translated following changes in sensory-driven activity. Given the extensive recurrent intracortical

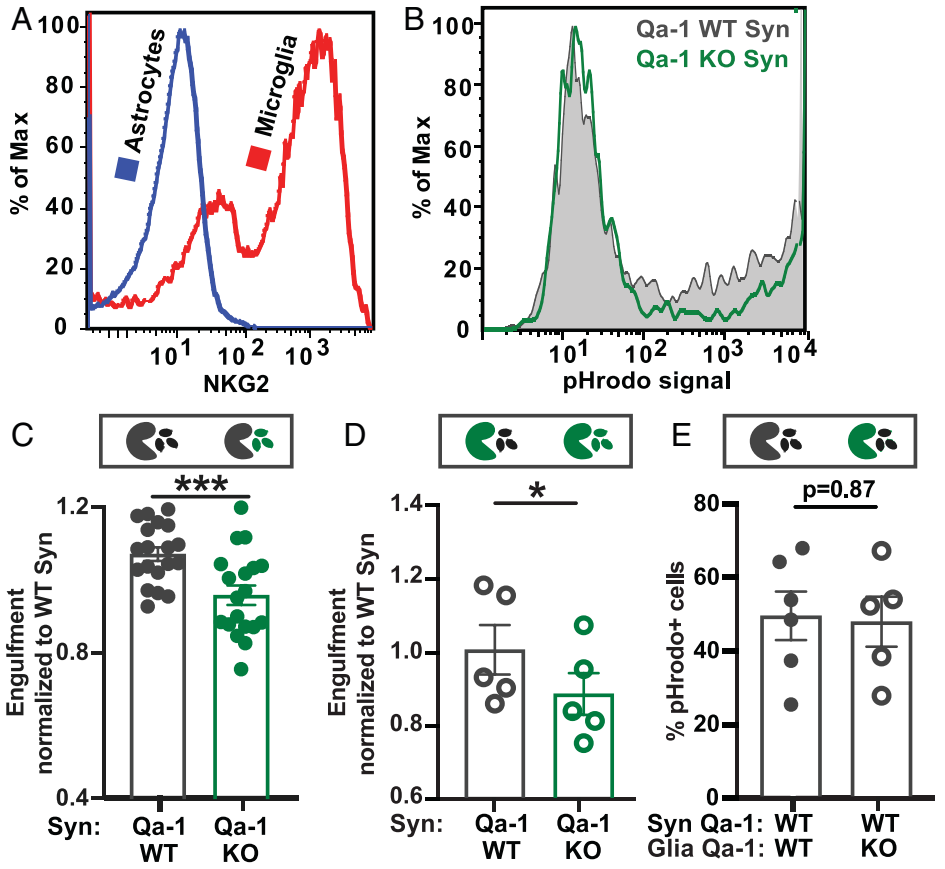

Fig. 6. Qa-1 contributes to microglial engulfment of synaptosomes *in vitro*. (*A*) FACS plot showing fluorescence intensity of NKG2 in cultured microglia (red) and astrocytes (blue). (*B*) Representative FACS plot showing fluorescence intensity of pHrodo-labeled cortical synaptosomes from Qa-1 WT (gray trace) and Qa-1 KO (green trace) mice, engulfed by WT microglia. (*C*–*E*) Mix-and-match experiments combining WT (black) or Qa-1 KO (green) microglia with WT or KO synaptosomes. (*C*) Quantification of the percentage Qa-1 WT microglia that engulf Qa-1 WT or KO synaptosomes (syn), normalized to WT engulfment ($n = 19$ WT mice used for cultures, from 5 independent experiments; each dot is average of 3 technical replicate cultures/animal). (*D*) Quantification of the percentage Qa-1 KO microglia that engulf WT or Qa-1 KO synaptosomes, normalized to WT engulfment ($n = 5$ KO mice used for cultures, from 2 independent experiments; each dot is average of 3 technical replicate cultures/animal). (*E*) Comparison showing a similar engulfment of WT synaptosomes by Qa-1 WT or KO microglia. ($n = 6$ WT and 5 KO mice used for cultures, from 2 independent experiments; each dot is average of 3 technical replicate cultures/animal) $^{*}P < 0.05$, $^{***}P < 0.001$, based on *t* test.

connections formed by L6 CT neurons with a variety of cell types in the sensory cortex (31, 33, 69), translation of Qa-1 mRNA could contribute to activity-dependent synaptic function in multiple cortical microcircuits.

Qa-1 Restricts the Extent of OD Plasticity in the Visual Cortex. In the absence of Qa-1, OD plasticity is dysregulated, as assessed by monitoring the expansion of territory representing the open eye in L4 and in L6 following MD using Arc mRNA induction (Fig. 4). Rather than finding no plasticity, unexpectedly, Qa-1 KO results in an even greater than normal expansion. Arc mRNA is rapidly up-regulated by neural activity and has been used in many studies to label neurons that are functionally linked to stimulation (8, 42, 51–53). Previous work using intrinsic signal imaging and evoked potential recordings has shown a good correlation between the expansion in width of Arc mRNA induction and the strengthening of visually driven responses via the open eye following MD (41, 43, 54), implying a role for Qa-1 in regulating the strengthening of the open eye. It is also notable that, within 4 d of MD, the expansion of Arc mRNA signal in both L4 and L6 is more extensive (~20%) in Qa-1 KO than in WT. Studies have shown that following MD in WT, the deprived eye input to cortical neurons rapidly weakens within 1 d via LTD, but major strengthening of the open eye input only occurs 5 to 6 d later (55, 56). This delay in open eye strengthening is also observed when Arc induction is used in WT mice as a readout for changes in open eye inputs to cortical neurons (43). Thus, this approach permits us to conclude that Qa-1 normally functions in OD plasticity by restricting the extent and rate of open eye strengthening in L4 and L6. To our knowledge, this neuronal function for a nonclassical MHCI molecule has not previously been reported.

Qa-1 May Act via CD94/NKG2 Expressed by Microglia. In the immune system, Qa-1 signals by interacting with innate immune receptors that are members of the NKG2 family (11, 57, 58). Here, we have shown that OD plasticity associated with open eye strengthening is phenocopied in the visual cortex of mice bearing a Qa-1 point mutation that blocks signaling to heterodimeric CD94/NKG2 receptors (Fig. 4 *D* and *E*). Multiple lines of evidence presented here (Fig. 5) suggest that microglia express both CD94 and NKG2, implicating them as signaling partners for neuronally expressed Qa-1. The NKG2 receptor family includes both activating (i.e., NKG2C) and inhibitory (i.e., NKG2A) receptor subunits (68). CD94 and NKG2 transcripts can be detected in cortical lysates. A subset of cortical microglia express NKG2 receptors, as detected using a panspecific NKG2 antibody for immunohistochemistry in cortical sections. To determine further which NKG2 family members are expressed, acute preparations were used to isolate microglia and query their NKG2 expression. Significant expression of NKG2C but not NKG2A

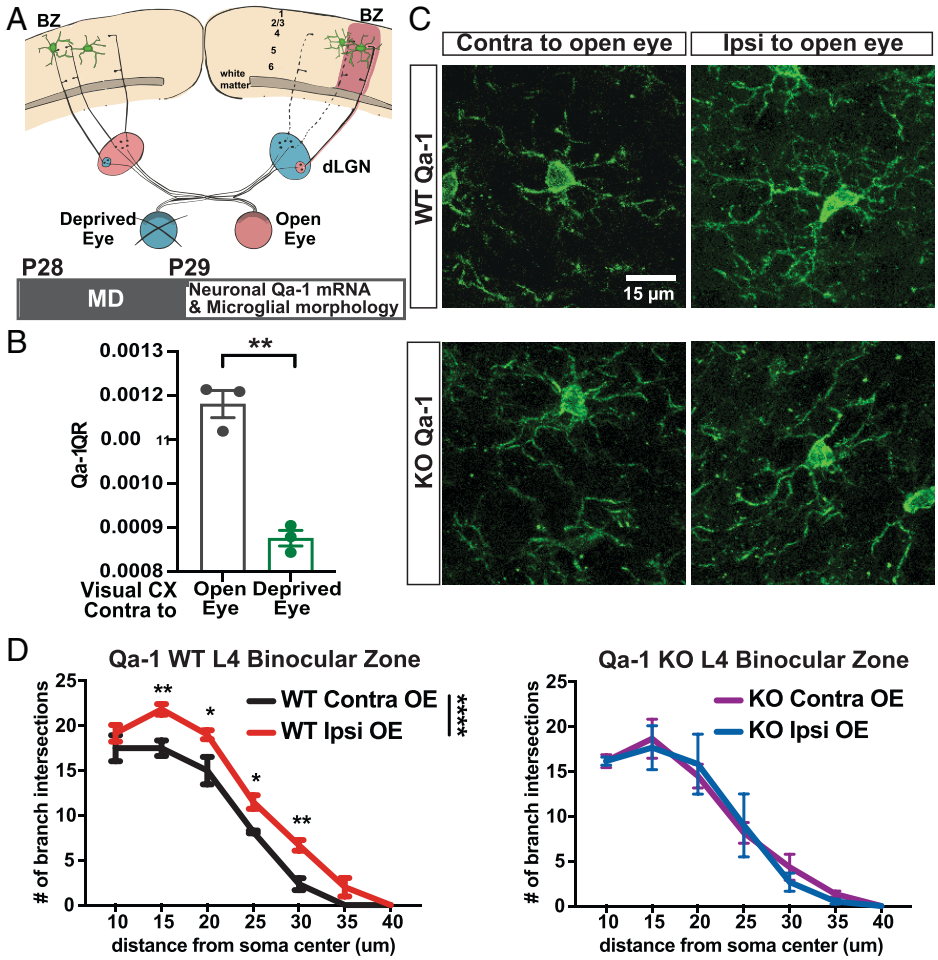

Fig. 7. A microglial response to monocular deprivation is impaired in Qa-1 KO mice. (*A*) Experimental paradigm showing MD at P28 followed by measurements of L6 Qa-1 neuronal transcripts and microglia morphology (in BZ of visual cortex) 24 h later. (*B*) qRT-PCR quantification of Qa-1 expression in L6 neurons of the visual cortex following 24 h of monocular deprivation. mRNA from the visual cortex contralateral to the open or closed eye was IP from Ntsr1-Cre x Ribotag mice. Expression levels are relative to GAPDH (n = 6 mice/group, visual cortices from 2 mice were pooled together per sample). (*C*) Representative images of microglia (immunostained for Iba1; scale, 15 µm) in L4 of BZ of WT versus Qa-1 KO cortex contralateral (*Left*) or ipsilateral (*Right*) to the open eye (24 h post-MD). (*D*) Sholl analysis of microglial process ramification in L4 BZ. *Top*, WT; *Bottom*, Qa-1 KO (n = 3 mice/group; 3 sections/mouse with at least 3 microglia/section). ****$P < 0.0001$, **$P < 0.01$, *$P < 0.05$, based on t tests (*B*) or two-way ANOVA with Tukey's post hoc (*D*).

was detected in microglia, suggesting that microglia express this particular family member. In NK cells, Qa-1 binding to NKG2C/CD94 results in downstream signaling and rapid reorganization of the actin cytoskeleton, consistent with the deficiency in the microglial morphological response to monocular deprivation seen in Qa-1 KO (67, 70, 71). We report here that microglia express the Qa-1 receptors CD94/NKG2, and previous studies have detected NKG2C mRNA in human and mouse brain [see Human Protein Atlas: gene name KLRC2, Tabula Muris Consortium (72)]. Together, these observations suggest that Qa-1-expressing L6 neurons might interact directly with CD94/NKG2C-expressing microglia at synapses to regulate activity-dependent plasticity, pointing to a fascinating avenue for future studies.

Activity-Dependent Changes in Microglial Morphology Require Qa-1. In the immune system, Qa-1 signaling via CD94/NKG2 can lead to changes in the cytoskeleton (67, 73). Here, we have observed that, in vivo, microglia fail to undergo the expected increase in process ramification following MD in L4 of the Qa-1 KO visual cortex, the target of the recurrent axonal projections of L6 neurons in the cortex (Fig. 7). This failure is also accompanied in vitro by a loss of synapse engulfment by microglia that depends upon Qa-1 expression in synaptosomes, rather than in microglia (Fig. 6). Both observations imply that neuronal Qa-1 contributes to changes in microglial morphology. Changes in microglial morphology are known to accompany, and may even be required, for intact OD plasticity via P2Y12 purinergic receptor expression in microglia (63). Electron microscopy studies of microglial interactions with synapses show that MD increases the number of contacts between microglia and synaptic profiles, as well as slightly increasing the number of GluA1-positive puncta and inclusions found within microglia (63). These changes could be part of the process of synaptic remodeling underlying the shift in OD that occurs during MD. In vivo imaging reveals that microglia actively probe and monitor neuronal processes (74), and studies have also noted that alterations in sensory experience can elicit morphological changes in extension and retraction of microglial processes without necessarily involving phagocytosis (75, 76).

It is worth noting that because Qa-1 is expressed almost exclusively in L6 neurons, the phenotypes that we have identified in Qa-1 and R72A mutant mice, including the microglial morphological changes, most likely depend upon this specific circuit. If so, how might the loss of Qa-1 function from L6 neurons generate an increase in open eye expansion and abrogate motility following MD? One possible explanation is that microglia fail to remove excitatory synapses belonging to L6 neurons in all relevant cortical layers including L4 and L6

because at these synapses Qa-1 is needed for microglia to detect sensory-driven changes in neural activity. The presence of additional L6 synapses in the Qa-1 KO cortex might in turn generate greater excitation from thalamic inputs driven by the open eye. While underlying mechanistic details remain to be fully elucidated, the observation that Qa-1 and its interaction with CD94/NKG2 in the cerebral cortex are needed for a properly regulated cortical response to changes in neural activity adds to a growing list of immune molecules involved in activity-dependent plasticity and synapse remodeling. This includes classical MHCI family members and the PirB receptor (8, 43, 77), components of the complement cascade (16), adenosine receptors (63), and multiple cytokines (78), and points to a remarkable evolutionary conservation of these molecules in both the brain and immune system.

Materials and Methods

Animals. All experiments involving animals were performed in accordance with guidelines and regulations approved by the Stanford University Animal Care and Use Committee. Qa-1^{KO} [25] and Qa-1^{R72A} [26] animals were received as a gift from the laboratory of Dr. Harvey Cantor (Harvard University) and maintained as an in-house colony. Ribotag [Rpl22-flox, Stock# 011029 (36)] and Snap25-Cre mice [Stock #023525 (35)] were obtained from Jackson Laboratories, while Ntsr1-Cre mice (34) were ordered from the Mutant Mouse Resource and Research Center (MMRRC) repository. The mice were maintained on a 12-h light/dark cycle with lights on at 7:00 AM. Experiments used littermate controls, and both male and female animals, as sex-dependent phenotypes were not observed. Investigators were not blinded to experimental group allocation, but quantifications were performed blind to experimental group.

Anesthesia. All surgeries (both survival and terminal) were performed with appropriate anesthesia. For monocular deprivation survival surgeries, the animals were initially anesthetized with 2.5% isoflurane and maintained under isoflurane (2.5%) for the remainder of the surgery. For terminal tissue collection surgeries where transcardial perfusions were not performed, animals were anesthetized with 3% isoflurane and decapitated immediately after. For tissue collection surgeries requiring transcardiac perfusion, animals were administered a lethal dose of Euthasol (Virbac) intraperitoneally (0.1 mL/animal).

RNAscope In Situ Hybridization. Animals were anesthetized with isoflurane (2.5%) as described in *Anesthesia*. Brains were rapidly collected and flash frozen in OCT Compound (Tissue-Tek). Brain slices were collected at 20-μm thickness on a cryostat set to −20 °C and immediately mounted on glass slides. Brains slices were stored at −80 °C until all brains from an experimental cohort were processed and ready for staining. Multiplex RNAscope was performed according to the manufacturer's protocol (ACD Bio, RNAscope Fluorescent Multiplex Assay) on a ACD HvbEZ II Hybridization System (110v) w/EZ-Batch Slide System. The probe for Qa-1 (Mm-H2T23-C1) was made to order and always in the C1 channel. Other probes used included the following: Mm-Slc17a7-C2 (VGluT1), m-Gad1-C3 (Gad1), Mm-Olig2-C2, Mm-Slc17a6-C2 (VGluT2), Mm-Fos-C3 (cFos), Mm-Arc-C3 (Arc), Mm-Slc1a3-C3 (EAAT1/Glast), Mm-Pecam1-C3 (CD31), and Cre-C2. Following staining, imaging was performed on a Leica SP8 confocal microscope (Leica Microsystems), using 20× magnification. Images were acquired at 1,024- × 1,024-pixel resolution in four color channels, corresponding to the three RNAscope fluorophores and DAPI. Next, 3 × 3 tile scans spanning the cortical layers were imaged together for stitching during postprocessing, and 15-μm z-stacks were acquired at each individual 20× field. Two sections per animal were imaged. For cell counting, intensity was summed across the z-direction in stitched z-stacks of images to produce a single projected image. Images were blinded by another researcher for manual cell counting. For quantification of Qa-1 mRNA expression in V1, three regions of interest (200 μm × 200 μm) in layer 6 were randomly selected to be quantified from each section. The total number of nuclei was quantified by applying a threshold to the DAPI staining and using the Analyze Particles function in Fiji (79). Colocalization of Qa-1 or other mRNA was then measured by manually counting the number of nuclei containing the fluorescence label. Nuclei counts were summed across regions of interest within each section and across sections for each animal. The overall proportion of cells that are Qa-1 positive was obtained by dividing the number of Qa-1+ DAPI-labeled nuclei by the total number of nuclei for each animal. The proportion of excitatory cells that are Qa-1 positive was obtained by dividing the number of Qa-1+, vGluT1+ DAPI-labeled nuclei by the number of vGluT1+ nuclei for each animal.

RNA Isolation and qRT-PCR. Animals were anesthetized with Euthasol as described in *Anesthesia* and perfused with heparinized phosphate-buffered saline (PBS), the brain was removed, and the cortex (or other brain regions, per experiment) was dissected and flash frozen. Samples were stored at −80 °C until all animals from an experimental cohort were processed. The tissue was homogenized by glass-bead beating for 30 s in 1 mL TRIzol (Invitrogen, 15596026), on a BeadBug homogenizer (E&K Scientific Products, 3110BX). The TRIzol extraction was then carried out according to the manufacturer's instructions and the RNA pellet resuspended in 20 to 100 μL (depending on input tissue size) molecular-grade water. For very small input tissue amounts, glycogen (at 0.05-μg/μL final solution) was added during the last spin in the RNA precipitation. The RNA was quantified, and DNA contamination removed using TURBO DNase (Invitrogen, AM2239), according to the manufacturer's instructions. The RNA was then diluted to even concentration across samples and converted to complementary DNA (cDNA) using the SensiFAST cDNA Synthesis Kit (Bioline, BIO65054), according to manufacturer's instructions and using no more than 1 μg input RNA. The resulting cDNA was then used for qRT-PCR reactions, using the SensiFAST SYBR No-ROX Kit (Bioline, BIO98005) and a BioRad CFX384 Touch Real-Time PCR Detection System. The following primer sequences were used: Arc - F: GAGCCTA CAGAGCCAGGAGA, R: GCAGCAAAGACTTCTCAGCA; H2-T23 – F: CGCGAATGACATA GCCTCACA, R: GCACCTCAGGGTGACTTCAT; Klrd1 – F: CTCATGGCAGTTTCTAGGATC AC, R: ACTGATGCCCAACCCACTTG; Klrc2v1 – F: CCAGAAGCATCTGAAGGCCA, R: ACAAGGCTGTGCTTTGGAGA; Klrc2v2 – F: CTCAGAACCCAGGAAAGCCA, R: AGGCTGT GATGGAGAAACAATTC; Klrc1 – F: GGAACCAGCACAGGAAACCA, R: GAAAACCTTTGC AGGGGCAAT; Tmem119 – F: GTGTCTAACAGGCCCCAGAA, R: AGCCACGTGGTATCAA GGAG; and Gapdh – F: AATGTGTCCGTCGTGGATCTGA, R: GATGCCTGCTTCACCAC CTTCT.

Ribotag Ribosome IP. Animals were anesthetized with isoflurane (2.5%) as described in *Anesthesia*. The brain was removed, and the cortex (or other brain regions) was dissected and either processed immediately or flash frozen. Ribotag IPs were carried out based on to the protocol in Sanz et al. (36) and Shigeoka et al. (40). Briefly, the tissue was submerged in cold 800 μL homogenization buffer (20 mM Hepes, 5 mM $MgCl_2$, 150 mM KCl, 1 mM DTT, 5 μL/mL RNasin, Complete EDTA-free Protease Inhibitor Mixture, 10% Nonidet P-40, and 0.2 mg/mL cycloheximide) and homogenized by 10 strokes in a 2-mL dounce homogenizer. The homogenate was then spun at 3,000 g for 10 min, at 4 °C, and the supernatant incubated with 5 μL anti-HA antibody (Abcam, 9110) for 4 h, with rotation at 4 °C. Protein A/G magnetic beads (Pierce, 88803) were then added and the samples further incubated overnight with rotation at 4 °C. The next morning, the beads were collected and washed twice with high salt buffer (50 mM Tris [pH 7.4], 300 mM KCl, 12 mM $MgCl_2$, and 10% Nonidet P-40), before being lysed in TRIzol, and RNA was isolated as described under *RNA Isolation and qRT-PCR*.

Synaptosome Isolation. Animals were anesthetized with isoflurane (2.5%) as described in *Anesthesia*. The brain was removed, and the cortex (or other brain regions) was dissected. Synaptosome-enriched fractions were isolated from freshly dissected cortices, based on previous protocols (80, 81). Tissue was submerged in cold isolation buffer (20 mM Hepes, 5 mM $MgCl_2$, 150 mM KCl, 1 mM DTT, 5 μL/mL RNasin, Complete EDTA-free Protease Inhibitor Mixture, and cycloheximide 0.2 mg/mL in 33% sucrose), and homogenized by 12 strokes using a 2-mL dounce homogenizer. The suspension was then centrifuged (10 min at 2,000 × *g* and 4 °C) and supernatants sequentially filtered through 70-μm and 40-μm membranes, followed by 5-μm nitrocellulose filters. Synaptosomes were collected by centrifugation at 10,000 × *g* for 10 min, washed with PBS nd then processed either for protein or RNA isolation (as described under *RNA Isolation and qRT-PCR*).

For microglial feeding experiments, the synaptosome pellet was weighed and resuspended at 10 μg/mL in 0.1 M sodium bicarbonate solution. Synaptosomes were then labeled with pHrodo Red (Invitrogen, P36600) for 30 to 40 min and washed twice with PBS, before being resuspended in PBS for feeding assays.

Western Blot and Analysis. For Western blot analysis of cortical tissue lysates and synaptosomes, samples were collected as described in *Synaptosome Isolation* and then quantified using a Bradford assay. Samples were then boiled for 5 min in the presence of sample buffer, and 4 to 5 μg was loaded onto a sodium dodecyl-sulfate polyacrylamide gel electrophoresis gel to undergo gel electrophoresis. Gels then were transferred onto a polyvinylidene fluoride membrane and blocked in 5% bovine serum albumin BSA for 1 h at room temperature (RT) and then placed in primary antibody overnight (α-PSD95, Neuromab 75-028, 1:500; α-synapsin, Abcam AB64581, 1:1,000; α-Tubulin, Abcam AB78078 1:2,000). The next day, blots were washed three times with 1× PBST (1× PBS + 0.1% Tween-20) for 5 min and incubated with Licor secondary antibodies for 2 h at RT. Blots were then washed in PBST and developed using the Licor Odyssey imaging system.

Visual Activity Manipulations. For dark exposure, animals were placed in a dark room for 10 d postweaning, starting at P21. Check-ups and cage changes were performed using night-vision goggles. Control animals were NR on a 12-h light/dark cycle. At the end of the dark exposure protocol, animals were either euthanized immediately after removal from the dark room or reexposed to ambient light for 5 to 10 h before tissue collection.

MD experiments were performed at P28 according to Datwani et al. (8). Animals were anesthetized with isoflurane (2.5%) and the left eyelids sutured shut before being returned to the home cage. For acute MD experiments, animals were euthanized and tissue collected 24 h postsurgery. For OD plasticity experiments, at P32, the left eyes in both MD and NR animals were enucleated to allow identification responses from the open eye only. After recovery, animals were placed in the dark room overnight to bring visually driven neuronal activity to baseline. The following morning, animals were removed from the dark and placed in a brightly lit room for 30 min in order to induce up-regulation of immediate early genes for binocular zone identification. Brains were collected immediately at the end of the 30-min period and flash frozen.

Histology and Immunohistochemistry. Animals were anesthetized with Euthasol as described in *Anesthesia*. Animals were intracardially perfused with heparinized (5 U/mL) PBS, followed by 4% paraformaldehyde (PFA). Brains were collected and postfixed for 24 to 48 h in 4% PFA, followed by cryoprotection in 30% sucrose for 48 h. Brains were flash frozen in OCT compound (Tissue-Tek) by dunking in 2-methyl-butane chilled on dry ice. Prior to being sliced, brains were acclimated in the chamber of a Leica cryostat set to −20 °C. Next, 40-μm sections were sliced into 24-well plates containing PBS with 0.05% sodium azide and stored at 4 °C until the entire cohort was ready for staining. For immunofluorescence, slices were permeabilized and endogenous epitopes blocked for 1 h at RT, in a solution containing 0.1% Triton X-100, 0.05% Tween-20, 1% BSA, and 2% serum of the secondary's species. Brain slices were then incubated overnight in 1% BSA + 0.1% Triton X-100 in PBS with primary antibody at 4 °C, followed by washes with PBS-Tween-20 (0.05%) and incubation in secondary antibody solution for 2 h at RT. After being thoroughly washed, slices were mounted with Aquamount (Thermo Scientific) or ProLong Gold (Thermo Scientific) and DAPI. The following antibodies were used for immunofluorescence staining: rabbit anti-Iba1 (1:1,000; FUJIFILM Wako, 019-19741), rat anti-NKG2A/C/E (1:500, BDBiosciences, 20d5), rat anti-CD94 (1:500, BDBiosciences, 18d3), and rabbit anti-HA (1:1,000, Abcam, 9110). Secondary antibodies were all from Life Technologies and used at 1:2,000. Following staining, imaging was performed on a Leica SP8 confocal microscope (Leica Microsystems), using 40× or 63× oil immersion objectives. Composite micrographs were assembled using Fiji (79). For microglia Sholl analyses the Linear Sholl Method Plugin for FIJI was used. Individual microglia were thresholded and Sholl shells were established in 5-μm intervals, 10 μm from the soma center to the longest observed process length. Representative images from at least three 40-μm sections of the visual cortex binocular zone were used, and at least three microglia were quantified per image.

Arc In Situ Hybridization. Animals were anesthetized with isoflurane (2.5%) as described in *Anesthesia*. The brain was removed and submerged in OCT Compound and then flash frozen on a slurry of dry ice and isopropanol. Arc in situ hybridization was performed as previously described (42, 82). Fresh-frozen slices (16 μm) were collected and hybridized with digoxigenin-labeled Arc antisense riboprobe for colorimetric reactions. Slices were then imaged on a brightfield microscope, and the width of Arc signal was measured in L4 and L6 using FIJI (79). Quantification was performed blind to treatment and genotype, and averaged from three to four slices per animal.

Adult Microglial Isolation. Animals were anesthetized with Euthasol as described in *Anesthesia*. Animals were perfused with heparinized PBS, the brain was removed, and the cortex was separated from subcortical structures. Cortices were gently homogenized by five strokes in MACS buffer, and resulting lysates were filtered through a 70-μm filter and washed to remove debris. The resulting pellet was resuspended in an isotonic 40% Percoll-PBS solution and centrifuged for 25 min at 1,150 rcf and 4 °C to remove myelin debris. The resulting pellet was washed in MACS buffer, and each sample was incubated for 15 min with 20 μL CD11b positive-selection beads (Miltenyi Biotec, 130-049-601) in MACS buffer (100-μL total volume). Cells were then loaded on positive-selection magnetic columns (Miltenyi Biotec, 130-042-401) and separation conducted according to the manufacturer's instructions. Cell suspensions from two cortices were loaded on one column and resulting fractions pooled into one unbound and one microglia fraction. A small aliquot of the resulting cell suspensions was prepared for microglia purity analysis by FACS. Following separation, cells were washed in MACS buffer and resuspended in TRIzol for RNA extraction.

Preparation of In Vitro Microglial Cultures and Engulfment Assays. Cortices were collected from P5 to P8 pups in DMEM/F12 buffered with Hepes (15mM), and subcortical structures and meninges were removed. The cortex from one animal was chopped using sharp forceps and digested in 1 mL papain (4U/mL) and DNase (50 U/mL) in Hank's balanced salt solution (HBSS, with cations) at 37 °C for 15 min. Each sample was triturated 10 times, filtered through a 70-μm filter, and washed with warm culture media (DMEM/F12 with 10% FBS and Anti-Anti). Pellets were resuspended in 15 mL of culture media and plated in T75 tissue-culture-treated flasks. A full media change was given ∼24 h after plating and half-medium changes ("feedings") were given after 1 wk and every third subsequent day.

Cells were collected after 2 wk by gentle scraping, washed, and prepared for FACS analysis. Staining was performed with an antibody mixture that included antibodies (1:1,000) against the following: CD45, CD11b, Glast, NKG2A/C/E (all from BD Biosciences), and Zombie-Aqua viability dye (BioLegend). The cells were analyzed on a Bio-Rad ZE5 Cell Analyzer.

Statistical Analyses. Statistical analyses were performed using Prism GraphPad. The appropriate statistical tests were chosen based on the number of experimental groups (*t* tests for two groups and ANOVAs for three or more groups, followed by Tuckey's post hoc tests). F tests were also performed, and Welch's corrections were applied when appropriate. The threshold for statistical significance was set at $P = 0.05$.

Data Availability. All study data are included in the article and/or *SI Appendix*.

ACKNOWLEDGMENTS. We thank the members of the C.J.S. laboratory for productive scientific discussion and feedback. Special thanks to N. Sotelo-Kury, P. Kemper, M. Stafford, and C. Chechelski for logistics, experimental support, and mouse breeding. We thank Dr. Harvey Cantor (Harvard Medical School) for providing Qa-1 KO and R72A transgenic mice and Dr. Alice Ting (Stanford University) and her laboratory for instruction in and use of their flow cytometer. This project was supported by NIH grants MH071666 and EY02858, the Champalimaud Foundation (C.J.S.), National Research Service Award F32 MH110066 (K.S.C.), the Good Ventures Foundation (I.A.M.), and the Stanford Bio-X Summer Undergraduate Program (A.Y.G.-W.).

Author affiliations: [a]Department of Biology, Stanford University, Stanford, CA 94035; and [b]Department of Neurobiology, Stanford University, Stanford, CA 94035

1. L. C. Katz, C. J. Shatz, Synaptic activity and the construction of cortical circuits. *Science* **274**, 1133–1138 (1996).
2. C. N. Levelt, M. Hübener, Critical-period plasticity in the visual cortex. *Annu. Rev. Neurosci.* **35**, 309–330 (2012).
3. T. A. Seabrook, T. J. Burbridge, M. C. Crair, A. D. Huberman, Architecture, function, and assembly of the mouse visual system. *Annu. Rev. Neurosci.* **40**, 499–538 (2017).
4. T. E. Faust, G. Gunner, D. P. Schafer, Mechanisms governing activity-dependent synaptic pruning in the developing mammalian CNS. *Nat. Rev. Neurosci.* **22**, 657–673 (2021).

5. A. D. Huberman, C. M. Speer, B. Chapman, Spontaneous retinal activity mediates development of ocular dominance columns and binocular receptive fields in v1. *Neuron* **52**, 247–254 (2006).
6. B. M. Hooks, C. Chen, Circuitry underlying experience-dependent plasticity in the mouse visual system. *Neuron* **106**, 21–36 (2020).
7. R. A. Corriveau, G. S. Huh, C. J. Shatz, Regulation of class I MHC gene expression in the developing and mature CNS by neural activity. *Neuron* **21**, 505–520 (1998).
8. A. Datwani *et al.*, Classical MHCI molecules regulate retinogeniculate refinement and limit ocular dominance plasticity. *Neuron* **64**, 463–470 (2009).
9. L. A. Needleman, X. B. Liu, F. El-Sabeawy, E. G. Jones, A. K. McAllister, MHC class I molecules are present both pre- and postsynaptically in the visual cortex during postnatal development and in adulthood. *Proc. Natl. Acad. Sci. U.S.A.* **107**, 16999–17004 (2010).
10. A. R. Mardinly *et al.*, Sensory experience regulates cortical inhibition by inducing IGF1 in VIP neurons. *Nature* **531**, 371–375 (2016).
11. V. M. Braud *et al.*, HLA-E binds to natural killer cell receptors CD94/NKG2A, B and C. *Nature* **391**, 795–799 (1998).
12. B. M. Elmer, A. K. McAllister, Major histocompatibility complex class I proteins in brain development and plasticity. *Trends Neurosci.* **35**, 660–670 (2012).
13. M. P. D'Souza *et al.*, Casting a wider net: Immunosurveillance by nonclassical MHC molecules. *PLoS Pathog.* **15**, e1007567 (2019).
14. M. W. Glynn *et al.*, MHCI negatively regulates synapse density during the establishment of cortical connections. *Nat. Neurosci.* **14**, 442–451 (2011).
15. J. D. Adelson *et al.*, Developmental sculpting of intracortical circuits by MHC class I H2-Db and H2-Kb. *Cereb. Cortex* **26**, 1453–1463 (2016).
16. A. H. Stephan, B. A. Barres, B. Stevens, The complement system: An unexpected role in synaptic pruning during development and disease. *Annu. Rev. Neurosci.* **35**, 369–389 (2012).
17. W. S. Chung *et al.*, Astrocytes mediate synapse elimination through MEGF10 and MERTK pathways. *Nature* **504**, 394–400 (2013).
18. I. D. Vainchtein *et al.*, Astrocyte-derived interleukin-33 promotes microglial synapse engulfment and neural circuit development. *Science* **359**, 1269–1273 (2018).
19. U. Neniskyte, C. T. Gross, Errant gardeners: Glial-cell-dependent synaptic pruning and neurodevelopmental disorders. *Nat. Rev. Neurosci.* **18**, 658–670 (2017).
20. L. Rajendran, R. C. Paolicelli, Microglia-mediated synapse loss in Alzheimer's disease. *J. Neurosci.* **38**, 2911–2919 (2018).
21. C. Madry, D. Attwell, Receptors, ion channels, and signaling mechanisms underlying microglial dynamics. *J. Biol. Chem.* **290**, 12443–12450 (2015).
22. G. S. Huh *et al.*, Functional requirement for class I MHC in CNS development and plasticity. *Science* **290**, 2155–2159 (2000).
23. M. M. Tetruashvily, J. W. Melson, J. J. Park, X. Peng, L. M. Boulanger, Expression and alternative splicing of classical and nonclassical MHCI genes in the hippocampus and neuromuscular junction. *Mol. Cell. Neurosci.* **72**, 34–45 (2016).
24. M. Chevée, J. J. Robertson, G. H. Cannon, S. P. Brown, L. A. Goff, Variation in activity state, axonal projection, and position define the transcriptional identity of individual neocortical projection neurons. *Cell Rep.* **22**, 441–455 (2018).
25. D. Hu *et al.*, Analysis of regulatory CD8 T cells in Qa-1-deficient mice. *Nat. Immunol.* **5**, 516–523 (2004).
26. L. Lu, H. J. Kim, M. B. Werneck, H. Cantor, Regulation of CD8+ regulatory T cells: Interruption of the NKG2A-Qa-1 interaction allows robust suppressive activity and resolution of autoimmune disease. *Proc. Natl. Acad. Sci. U.S.A.* **105**, 19420–19425 (2008).
27. C. C. Oliveira *et al.*, The nonpolymorphic MHC Qa-1b mediates CD8+ T cell surveillance of antigen-processing defects. *J. Exp. Med.* **207**, 207–221 (2010).
28. J. Ding *et al.*, Systematic comparison of single-cell and single-nucleus RNA-sequencing methods. *Nat. Biotechnol.* **38**, 737–746 (2020).
29. A. B. Rosenberg *et al.*, Single-cell profiling of the developing mouse brain and spinal cord with split-pool barcoding. *Science* **360**, 176–182 (2018).
30. Y. Zhou *et al.*, Human and mouse single-nucleus transcriptomics reveal TREM2-dependent and TREM2-independent cellular responses in Alzheimer's disease. *Nat. Med.* **26**, 131–142 (2020).
31. D. S. Bortone, S. R. Olsen, M. Scanziani, Translaminar inhibitory cells recruited by layer 6 corticothalamic neurons suppress visual cortex. *Neuron* **82**, 474–485 (2014).
32. E. M. Callaway, J. L. Lieber, Development of axonal arbors of layer 6 pyramidal neurons in ferret primary visual cortex. *J. Comp. Neurol.* **376**, 295–305 (1996).
33. J. Kim, C. J. Matney, A. Blankenship, S. Hestrin, S. P. Brown, Layer 6 corticothalamic neurons activate a cortical output layer, layer 5a. *J. Neurosci.* **34**, 9656–9664 (2014).
34. S. Gong *et al.*, Targeting Cre recombinase to specific neuron populations with bacterial artificial chromosome constructs. *J. Neurosci.* **27**, 9817–9823 (2007).
35. J. A. Harris *et al.*, Anatomical characterization of Cre driver mice for neural circuit mapping and manipulation. *Front. Neural Circuits* **8**, 76 (2014).
36. E. Sanz *et al.*, Cell-type-specific isolation of ribosome-associated mRNA from complex tissues. *Proc. Natl. Acad. Sci. U.S.A.* **106**, 13939–13944 (2009).
37. V. Rangaraju, S. Tom Dieck, E. M. Schuman, Local translation in neuronal compartments: How local is local? *EMBO Rep.* **18**, 693–711 (2017).
38. D. Merkurjev *et al.*, Synaptic N^6-methyladenosine (m^6A) epitranscriptome reveals functional partitioning of localized transcripts. *Nat. Neurosci.* **21**, 1004–1014 (2018).
39. C. E. Holt, K. C. Martin, E. M. Schuman, Local translation in neurons: Visualization and function. *Nat. Struct. Mol. Biol.* **26**, 557–566 (2019).
40. T. Shigeoka *et al.*, Dynamic axonal translation in developing and mature visual circuits. *Cell* **166**, 181–192 (2016).
41. J. Cang, V. A. Kalatsky, S. Löwel, M. P. Stryker, Optical imaging of the intrinsic signal as a measure of cortical plasticity in the mouse. *Vis. Neurosci.* **22**, 685–691 (2005).
42. Y. Tagawa, P. O. Kanold, M. Majdan, C. J. Shatz, Multiple periods of functional ocular dominance plasticity in mouse visual cortex. *Nat. Neurosci.* **8**, 380–388 (2005).
43. M. Djurisic *et al.*, PirB regulates a structural substrate for cortical plasticity. *Proc. Natl. Acad. Sci. U.S.A.* **110**, 20771–20776 (2013).
44. T. K. Hensch, E. M. Quinlan, Critical periods in amblyopia. *Vis. Neurosci.* **35**, E014 (2018).
45. M. Majdan, C. J. Shatz, Effects of visual experience on activity-dependent gene regulation in cortex. *Nat. Neurosci.* **9**, 650–659 (2006).
46. D. Tropea, A. Van Wart, M. Sur, Molecular mechanisms of experience-dependent plasticity in visual cortex. *Philos. Trans. R. Soc. Lond. B Biol. Sci.* **364**, 341–355 (2009).
47. N. Picard *et al.*, Aberrant development and plasticity of excitatory visual cortical networks in the absence of cpg15. *J. Neurosci.* **34**, 3517–3522 (2014).
48. F. Briggs, Organizing principles of cortical layer 6. *Front. Neural Circuits* **4**, 3 (2010).
49. T. D. Mrsic-Flogel *et al.*, Homeostatic regulation of eye-specific responses in visual cortex during ocular dominance plasticity. *Neuron* **54**, 961–972 (2007).
50. S. B. Hofer, T. D. Mrsic-Flogel, T. Bonhoeffer, M. Hübener, Experience leaves a lasting structural trace in cortical circuits. *Nature* **457**, 313–317 (2009).
51. S. Chowdhury *et al.*, Arc/Arg3.1 interacts with the endocytic machinery to regulate AMPA receptor trafficking. *Neuron* **52**, 445–459 (2006).
52. D. K. Bilkey *et al.*, Exposure to complex environments results in more sparse representations of space in the hippocampus. *Hippocampus* **27**, 1178–1191 (2017).
53. G. Vetere *et al.*, Chemogenetic interrogation of a brain-wide fear memory network in mice. *Neuron* **94**, 363–374.e4 (2017).
54. C. M. William *et al.*, Synaptic plasticity defect following visual deprivation in Alzheimer's disease model transgenic mice. *J. Neurosci.* **32**, 8004–8011 (2012).
55. M. Y. Frenkel, M. F. Bear, How monocular deprivation shifts ocular dominance in visual cortex of young mice. *Neuron* **44**, 917–923 (2004).
56. G. B. Smith, A. J. Heynen, M. F. Bear, Bidirectional synaptic mechanisms of ocular dominance plasticity in visual cortex. *Philos. Trans. R. Soc. Lond. B Biol. Sci.* **364**, 357–367 (2009).
57. R. E. Vance, A. M. Jamieson, D. H. Raulet, Recognition of the class Ib molecule Qa-1(b) by putative activating receptors CD94/NKG2C and CD94/NKG2E on mouse natural killer cells. *J. Exp. Med.* **190**, 1801–1812 (1999).
58. H. J. Pegram, D. M. Andrews, M. J. Smyth, P. K. Darcy, M. H. Kershaw, Activating and inhibitory receptors of natural killer cells. *Immunol. Cell Biol.* **89**, 216–224 (2011).
59. J. C. Cronk *et al.*, Peripherally derived macrophages can engraft the brain independent of irradiation and maintain an identity distinct from microglia. *J. Exp. Med.* **215**, 1627–1647 (2018).
60. A. S. Rapaport *et al.*, The inhibitory receptor NKG2A sustains virus-specific $CD8^+$ T cells in response to a lethal poxvirus infection. *Immunity* **43**, 1112–1124 (2015).
61. D. P. Schafer *et al.*, Microglia sculpt postnatal neural circuits in an activity and complement-dependent manner. *Neuron* **74**, 691–705 (2012).
62. E. K. Lehrman *et al.*, CD47 protects synapses from excess microglia-mediated pruning during development. *Neuron* **100**, 120–134.e6 (2018).
63. G. O. Sipe *et al.*, Microglial P2Y12 is necessary for synaptic plasticity in mouse visual cortex. *Nat. Commun.* **7**, 10905 (2016).
64. R. C. Paolicelli, K. Bisht, M. È. Tremblay, Fractalkine regulation of microglial physiology and consequences on the brain and behavior. *Front. Cell. Neurosci.* **8**, 129 (2014).
65. C. J. Bohlen *et al.*, Diverse requirements for microglial survival, specification, and function revealed by defined-medium cultures. *Neuron* **94**, 759–773.e8 (2017).
66. A. D. Umpierre *et al.*, Microglial calcium signaling is attuned to neuronal activity in awake mice. *eLife* **9**, e56502 (2020).
67. K. Lagrue *et al.*, The central role of the cytoskeleton in mechanisms and functions of the NK cell immune synapse. *Immunol. Rev.* **256**, 203–221 (2013).
68. P. M. Saunders *et al.*, A bird's eye view of NK cell receptor interactions with their MHC class I ligands. *Immunol. Rev.* **267**, 148–166 (2015).
69. J. E. Frandolig *et al.*, The synaptic organization of layer 6 circuits reveals inhibition as a major output of a neocortical sublamina. *Cell Rep.* **28**, 3131–3143.e5 (2019).
70. L. L. Lanier, B. Corliss, J. Wu, J. H. Phillips, Association of DAP12 with activating CD94/NKG2C NK cell receptors. *Immunity* **8**, 693–701 (1998).
71. H. L. Hoare *et al.*, Subtle changes in peptide conformation profoundly affect recognition of the non-classical MHC class I molecule HLA-E by the CD94-NKG2 natural killer cell receptors. *J. Mol. Biol.* **377**, 1297–1303 (2008).
72. Tabula Muris Consortium; Overall coordination; Logistical coordination; Organ collection and processing; Library preparation and sequencing; Computational data analysis; Cell type annotation; Writing group; Supplemental text writing group; Principal investigators, Single-cell transcriptomics of 20 mouse organs creates a Tabula Muris. *Nature* **562**, 367–372 (2018).
73. X. Chen, P. P. Trivedi, B. Ge, K. Krzewski, J. L. Strominger, Many NK cell receptors activate ERK2 and JNK1 to trigger microtubule organizing center and granule polarization and cytotoxicity. *Proc. Natl. Acad. Sci. U.S.A.* **104**, 6329–6334 (2007).
74. A. Nimmerjahn, F. Kirchhoff, F. Helmchen, Resting microglial cells are highly dynamic surveillants of brain parenchyma in vivo. *Science* **308**, 1314–1318 (2005).
75. M. È. Tremblay, R. L. Lowery, A. K. Majewska, Microglial interactions with synapses are modulated by visual experience. *PLoS Biol.* **8**, e1000527 (2010).
76. L. Cheadle *et al.*, Sensory experience engages microglia to shape neural connectivity through a non-phagocytic mechanism. *Neuron* **108**, 451–468.e9 (2020).
77. J. Syken, T. Grandpre, P. O. Kanold, C. J. Shatz, PirB restricts ocular-dominance plasticity in visual cortex. *Science* **313**, 1795–1800 (2006).
78. I. Marin, J. Kipnis, Learning and memory ... and the immune system. *Learn. Mem.* **20**, 601–606 (2013).
79. J. Schindelin *et al.*, Fiji: An open-source platform for biological-image analysis. *Nat. Methods* **9**, 676–682 (2012).
80. M. W. Johnson, J. K. Chotiner, J. B. Watson, Isolation and characterization of synaptoneurosomes from single rat hippocampal slices. *J. Neurosci. Methods* **77**, 151–156 (1997).
81. C. J. Westmark, P. R. Westmark, Preparation of synaptoneurosomes for the study of glutamate receptor function. *Methods Mol. Biol.* **1941**, 189–197 (2019).
82. D. N. Bochner *et al.*, Blocking PirB up-regulates spines and functional synapses to unlock visual cortical plasticity and facilitate recovery from amblyopia. *Sci. Transl. Med.* **6**, 258ra140 (2014).